(Received 11 March 2024, Accepted 30 April 2024, Scheduled 21 May 2024)

Metamaterial-Based Compact UWB Bandpass Filter Using Substrate Integrated Waveguide

Senathipathi Udhayanan and Krishnan Shambavi*

School of Electronics Engineering, Vellore Institute of Technology, Vellore, India

ABSTRACT: A compact ultra-wideband (UWB) bandpass filter is realized with the combination of dual-split square complementary split ring resonator (DSS-CSRR) and substrate integrated waveguide and is investigated in this paper. Three DSS-CSRRs are carved on the top and bottom layers of SIW to achieve the required passband and enhance the selectivity of the filter. Slots are etched in the ground to improve the return loss characteristics and to lower the insertion loss. The proposed filter offers a fractional bandwidth of 107% (3.1–10.3 GHz) and an insertion loss range of 0.6–1.6 dB in the entire passband. The prototype was fabricated on an FR-4 substrate, with dimensions of $0.35\lambda_g L \times 1.06\lambda_g W$. The group delay variation is almost flat over the entire passband. The prototype was fabricated and validated the measured results.

1. INTRODUCTION

Ultra-wideband (UWB) technology has recently gained popularity because it can transfer data quickly and offer trustworthy communications for industries such as telecommunications, aerospace, and military. The purpose of UWB bandpass filters is to eliminate undesired signals and noise in UWB applications [1, 2]. Nowadays, researchers mainly focus on compact and low-profile filters for space-constrained applications and easy-to-integrate existing applications. These filters can be implemented using different transmission lines, like microstrip lines, strip lines, rectangular waveguides, etc. Due to the high radiation loss and ohmic loss, the typical microstrip filter results in high insertion loss in the passband [3]. Furthermore, the quality factor is also not reasonable compared to a traditional rectangular waveguide; that structure is bulkier and more expensive. The planar technology-based substrate-integrated waveguide (SIW) has a similar characteristic to that of a traditional rectangular waveguide. The primary benefits of SIW are its high-power handling capabilities, ease of integration with planar components, and inexpensive fabrication cost.

To achieve compactness and improve the performance standard of the microwave filters, metamaterials such as split ring resonator (SRR) and complementary SRR (CSRR) are added to SIW. SRR features a strong rejection band because of its negative permeability and complementary structure of SRR or CSRR, which gives negative permittivity close to its resonance frequency. CSRRs are sub-lambda structures [4, 5]; their dimensions are relatively small at the resonance frequency, which is one-tenth of the guide wavelength. Hence, the high level of miniaturization is expected using this metamaterial structure [6–8]. Furthermore, SRR-loaded waveguide provides a stopband when it resonates below the waveguide cutoff frequency. Similarly, CSRR provides a stopband above the waveguide cutoff. According to the theory of evanescent mode, the additional passband below the cutoff can be obtained by loading CSRRs [9–11]. Many single and dual-band filters have been implemented using SRRs. CSRR-loaded SIW filters were reported in [12–14] to miniaturize the filter structure.

In this work, a SIW-based UWB bandpass filter designed using a dual-split square complementary split ring resonator (DSS-CSRR) to enhance the coupling is presented. The DSS-CSRR was etched on the top and ground layers to obtain the required passband characteristics and to enhance the selectivity. The slots were introduced in the ground layer to compensate the impedance variation. The designed filter has UWB, low insertion loss, and miniaturized size. Hence, it is well suited for space applications.

2. FILTER DESIGN AND ANALYSIS

2.1. Design of SIW Structure

SIW and conventional rectangular waveguides have similar mode characteristics. In SIW, periodic vias are utilized to realize side walls, and the separation between the vias should satisfy (1) and (2) to minimize the leakage loss, where p is the separation between the vias,

$$p \leq 2d \tag{1}$$

$$0.05 \leq \frac{p}{\lambda_c} \leq 0.25 \tag{2}$$

The waveguide's cutoff wavelength is represented by λ_c, whereas d represents the diameter of the vias. SIW behaves as a high-pass filter, and its cutoff frequency depends on the effective separation between the two-side walls of SIW (W_W), which can be calculated using (3) and (4). Here, W is the actual width of the waveguide; ε_r and c represent the dielectric

* Corresponding author: Krishnan Shambavi (kshambavi@vit.ac.in).

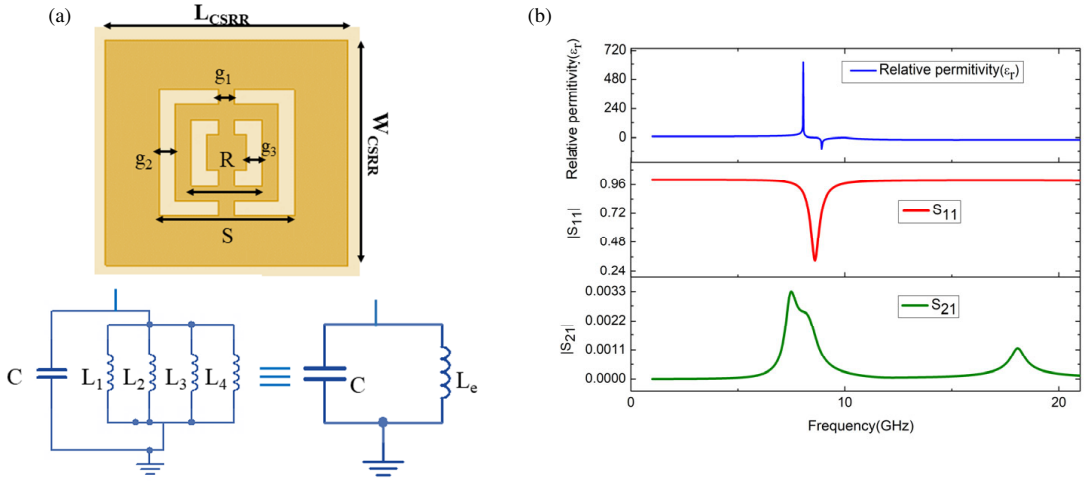

FIGURE 1. (a) Unit cell of CSRR and their lumped circuit. (b) Permittivity of DS-CSRR unit cell.

constant of the substrate and velocity of light in free space, respectively.

$$f_c = \frac{c}{2W_W\sqrt{\varepsilon_r}} \tag{3}$$

$$W_W = W - 1.08\,\frac{d^2}{p} + 0.1\,\frac{d^2}{W} \tag{4}$$

The dimensions of the proposed unloaded SIW filter realized on an FR-4 substrate with a relative permittivity of 4.3 and a height of 1.6 mm are $p = 1.5$ mm, $d = 0.8$ mm, $W = 20.88$ mm, $W_W = 20.08$ mm, $L_W = 7.5$ mm, $F_W = 2.7$ mm, $T_W = 4.4$ mm, $F_L = 1.85$ mm, $T_L = 1.90$ mm, respectively. The overall dimension of the filter is $15 \times 22.3 \times 1.6$ mm^3. The cutoff frequency of the SIW structure is 12.2 GHz. It can be controlled by altering the waveguide width (W_W).

2.2. Design of CSRR

CSRR provides a negative permittivity at the resonance frequency and generates an abrupt rejection band around the designed frequency. In this proposed SIW filter, a novel dual-split square CSRR of 8.45 GHz resonant frequency is implemented to obtain the desired wideband characteristics. The geometry of a dual-split square CSRR etched on an FR-4 substrate and its equivalent circuit are shown in Fig. 1(a). The full-wave electromagnetic simulation of the DSS-CSRR was carried out using computer simulation technology (CST) software. The optimized dimensions are $W_{\text{CSRR}} = L_{\text{CSRR}} = 7.5$ mm, $R = 2.2$ mm, $S = 4.2$ mm, $g_1 = g_2 = g_3 = 0.5$ mm. The equivalent inductance (L_e) and capacitance (C) extracted from the full-wave numerical simulation are 8.19 nH and 0.043 pF, respectively. Fig. 1(b) depicts the unit cell characteristics of dual-split square CSRR. The band reject frequency of the unit cell is 8.45 GHz, and its negative permittivity is high at the resonant frequency. By incorporating this resonator into the unloaded SIW filter, the band edge characteristics of the bandpass filter can be tuned to obtain the required bandwidth.

2.3. Design and Analysis of Proposed UWB Filter

A 50 Ω microstrip line, followed by a tapered section acts as a feed to the SIW filter. The length of the tapered section depends on quarter wavelength, and width can be calculated using Equation (5) to match the impedance between waveguide and feedline.

$$Z = \frac{60}{\sqrt{\varepsilon_e}}\,\ln\left(8\,\frac{h}{T_w} + 0.25\,\frac{T_w}{h}\right) \tag{5}$$

where Z — waveguide impedance, T_w — flaring width, and h, ε_e represent the height and effective permittivity of the substrate, respectively. The CSRR carved on the top and bottom layers acts as a resonator and controls the upper band edge characteristics. The slots are etched in the bottom layer to maintain a proper matching in the passband. The resonant modes depend on the size of the unit cell structure. Fig. 2 shows the evolution and corresponding frequency response characteristics of the proposed UWB filter.

By incorporating dual split-CSRR on the top layer, it exhibits wideband characteristics with 3 dB cutoff frequencies of 3.1 GHz and 12.1 GHz (Fig. 2(a)). Introducing the CSRR in the ground plane (Fig. 2(b)) changes the filter's resonance frequency by lowering the upper cutoff frequency from 12 GHz to 10.3 GHz. Loading CSRRs on both layers of SIW changes the overall impedance, which affects the insertion and return loss characteristics. Hence, the slots are etched in the ground plane to compensate for the variation (Fig. 2(c)). A triangular slot in the ground plane enhances the stopband attenuation with the maximum stopband attenuation of −73 dB at 15 GHz. The overall stopband attenuation is greater than 20 dB and is main-

TABLE 1. Performance summary of proposed SIW-BPF.

Parameter	*Simulated*	*Measured*
Centre frequency f_0 (GHz)	6.8	6.55
Insertion loss (dB) @f_0	1.64	2.3
Max. Return loss (dB) in passband	−30	−36
Fractional bandwidth (%)	107	105
Stopband Rejection (dB) @15 GHz	−70	−55

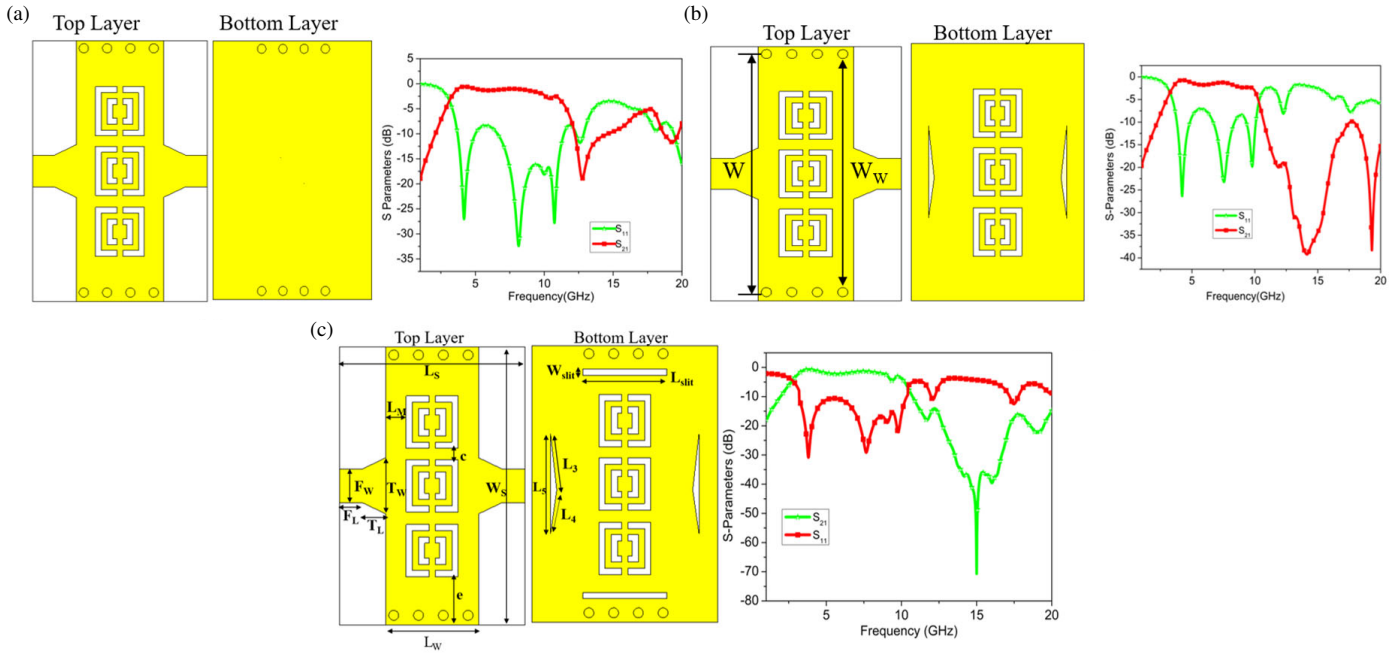

FIGURE 2. Design stages of UWB bandpass filter. The geometrical parameters of the filter is: $F_w = 2.7$, $F_L = 1.85$, $T_L = 1.90$, $T_w = 4.4$, $L_M = 1.7$, $L_W = 7.5$, $L_s = 15$, $W_S = 22.3$, $W_s = 22.3$, $e = 3.8$, $c = 1$, $W_{\text{slit}} = 0.5$, $p = 2$, $d = 0.8$, $L_3 = 4.53$, $L_4 = 3.54$, $L_5 = 8$, $L_{\text{slit}} = 6.8$, and $L_{\text{CSRR}} = 7.5$, respectively. (Unit: mm).

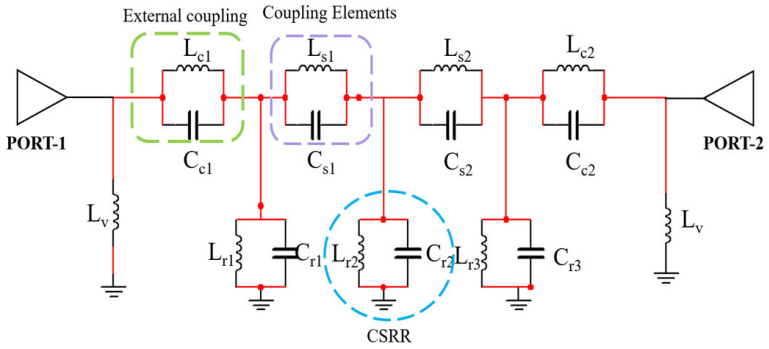

FIGURE 3. Equivalent circuit of proposed filter. The element values are: $L_{C1} = 4.66\,\text{nH}$, $C_{C1} = 0.893\,\text{pF}$, $L_{S1} = 1.35\,\text{nH}$, $C_{S1} = 0.057\,\text{pF}$, $L_{C2} = 3.83\,\text{nH}$, $C_{C2} = 0.955\,\text{pF}$, $L_{S2} = 1.23\,\text{nH}$, $C_{S2} = 0.089\,\text{pF}$ $L_{r1} = 4.17\,\text{nH}$, $C_{r1} = 0.145\,\text{pF}$, $L_{r2} = 6.4\,\text{nH}$, $C_{r2} = 0.38\,\text{pF}$, $L_{r3} = 4.99\,\text{nH}$, $C_{r3} = 0.165\,\text{pF}$, $L_V = 3.92\,\text{nH}$.

tained up to 18.2 GHz. The horizontal slot improves the return loss characteristics and helps to increase the stopband attenuation and selectivity of the filter. Hence, the designed filter exhibits an insertion loss of 1.3 dB at 5.3 GHz and a minimum insertion loss of 0.6 dB at 3.5 GHz. The overall optimized filter dimensions are depicted in Fig. 2(c).

2.4. Equivalent Circuit Model

Figure 3 shows the equivalent circuit model that explains the transmission characteristics of the proposed UWB filter. The SIW acts as a two-wire transmission line (considered as the top metal layer and ground layer) and is loaded with infinite via walls, considered as a short-circuited stub. These vias are considered as an inductor L_v. The CSRR is modelled as a tank circuit formed by capacitor C_r and inductor L_r. L_c and C_c indicate the inductive and capacitive coupling between the waveguide transmission line and CSRR, while L_s and C_s indicate the inductive and capacitive coupling between the CSRRs. The strong electric and magnetic field coupling between the waveguide and resonator is depicted in Fig. 5(b). The coupling inductance and capacitance values via inductance are calculated by using the following formulas,

$$L_C = \mu_0 \left(\frac{W_w}{2\pi}\right) \log\left[csc\left(\frac{\pi L_M}{2W_w}\right)\right] \tag{6}$$

$$C_C = \varepsilon_0 \varepsilon_{eff} \left(\frac{2W_w}{\pi}\right) \log\left[csc\left(\frac{\pi g}{2W_w}\right)\right] \tag{7}$$

$$L = 5.08h\left[\ln\left(\frac{4h}{d}\right) + 1\right] \text{ nH} \tag{8}$$

TABLE 2. Comparison with other wideband SIW bandpass filters.

Ref.	f_0 (GHz)	Size (λ_g^2)/Technique	Passband Range (GHz)	3 dB FBW (%)	IL	Upper Stopband
[1]	6.62	0.33/Microstrip	2.15–11.1	132	< 1.6	12 dB @2.78f_0
[2]	4.08	0.29/Microstrip	2.05–6.12	99.6	< 1.7	10 dB @2.21f_0
[8]	8.52	0.78/SIW	6.75–10.3	42	< 1.1	20 dB @1.8f_0
[10]	6.3	0.56/Microstrip	2.6–10.0	108	< 2.1	15 dB @2.21f_0
[11]	6.85	0.56/SIW	3.1–10.6	109	< 1.2	15 dB @2.05f_0
[12]	6.87	0.39/SIW	2.9–10.85	115	< 1	20 dB @2.9f_0
[13]	6.97	0.68/Microstrip	3.25–10.7	107	< 0.5	20 dB @2.45f_0
This Work	6.7	0.37/SIW	3.1–10.3	107	< 1.6	15 dB @2.72f_0

f_0: Centre frequency; λ_g: guided wavelength at the center frequency of passband;
FBW: Fractional Bandwidth; IL: Insertion Loss (dB)

where ε_0 and μ_0 are permittivity and permeability of free space, respectively; ε_{eff} is the effective permittivity; W_w is the waveguide width; and L_M represents the gap between CSRR and feed position which is shown in Fig. 2. h indicates the height of the substrate, and d indicates the diameter of the via (unit in inches). Fig. 4 shows the comparison between EM simulation and circuit simulation of the designed SIW bandpass filter, which are executed by CST and ADS software. The external coupling between SIW and CSRR creates a transmission zero at low frequency. The transmission zero was created at high frequency due to the coupling between CSRRs.

The circuit exhibits wideband characteristics (Fig. 4). The resonant modes f_1, f_2, and f_3 in the passband are produced by the resonators to enhance filter bandwidth. The 3 dB bandwidth ranges from 3.1 GHz to 10 GHz with a fractional bandwidth of 105% and an insertion loss of 0.04–0.565 dB. The stopband attenuation is $\geq$ 40 dB up to 20 GHz.

2.5. Surface Current and Field Distribution

The surface current distributions for passband and stopband are delineated in Fig. 5. The surface currents at 1 GHz and 15 GHz (Fig. 5(a)) represent the stopband characteristics. Here, there is no current flow between port 1 and port 2 and vice versa. From this current distribution, a stopband at 1 GHz is created due to the evanescent mode characteristics of the filter. However, at 15 GHz, the attenuation is generated due to the triangular slot in the ground plane.

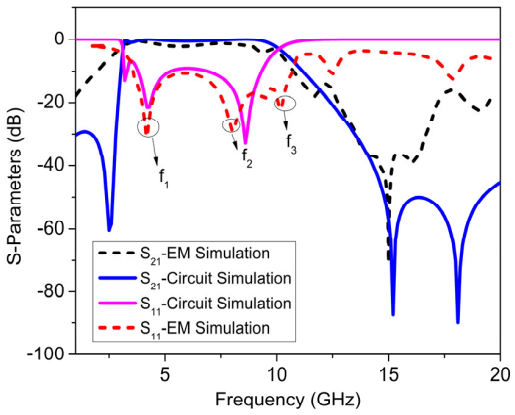

FIGURE 4. S-parameter of circuit simulation and EM simulation.

3. FABRICATION AND MEASUREMENT RESULTS

3.1. Fabrication and Measurement Results

Figure 6 shows the measurement setup and fabricated prototype. The S-parameter and group delay measurements are carried out using the vector network analyzer Anritsu-MS2027C. The comparison of measured and simulated outcomes is shown in Fig. 7. The measured passband ranges from 2.94 to 9.8 GHz, with a maximum in-band insertion loss of 2.3 dB and return loss better than -7 dB. A good agreement exists between simulated and measured results. The fractional bandwidth of 105% is obtained for the center frequency of $f_{0\text{UWB}}$ at 6.55 GHz. The measured results offer upper-stopband attenuation of $\geq$ 20 dB up to 18.2 GHz. The lower and upper band transmission zeros are obtained at 1.07 GHz and 15 GHz, which enhances the filter selectivity reasonably. Meanwhile, three reflection zeros are generated in the passband at 3.8 GHz, 7.65 GHz, and 9.7 GHz, which helps wideband creation. Due to the VNA frequency range limitations, the measurements are carried out up to 15 GHz. The small deviations in the measured results correspond to fabrication tolerance and connector loss. Table 1 summarizes the simulated and measured performance of the proposed filter. Table 2 compares similar works reported recently, and it is observed that our design features a compact size, wide bandwidth, and wide stopband attenuation.

3.2. Group Delay

Figure 8 shows the group delay over the passband which is almost constant. Hence, the linearity between the input and output is maintained over the passband. From the group delay of S_{11}, the external quality factor Q_e can also be calculated us-

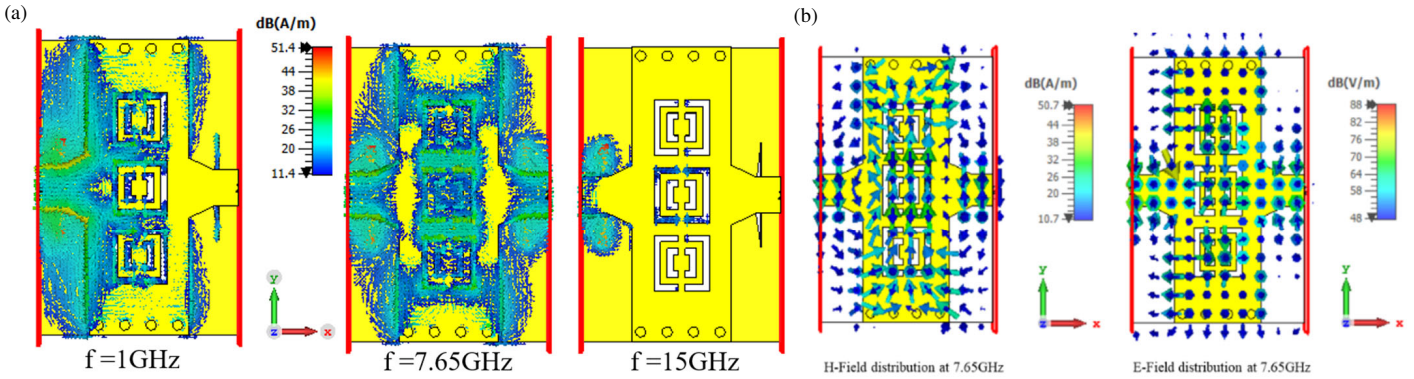

FIGURE 5. (a) Current distributions at different frequencies $f = 1$ GHz (Stopband), 7.65 GHz (Passband), and 15 GHz (Stopband). (b) E-field and H-field distributions at 7.65 GHz.

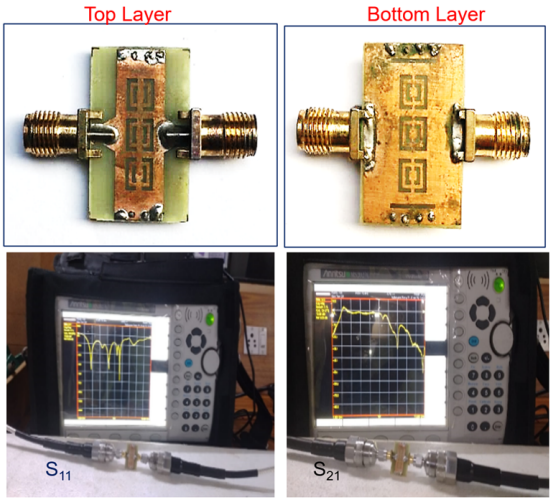

FIGURE 6. Measurement setup and prototype of proposed UWB SIW bandpass filter.

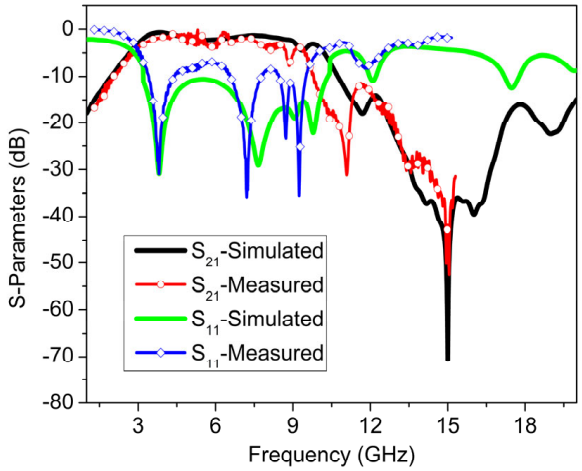

FIGURE 7. Measured and simulated S-parameters of proposed UWB filter.

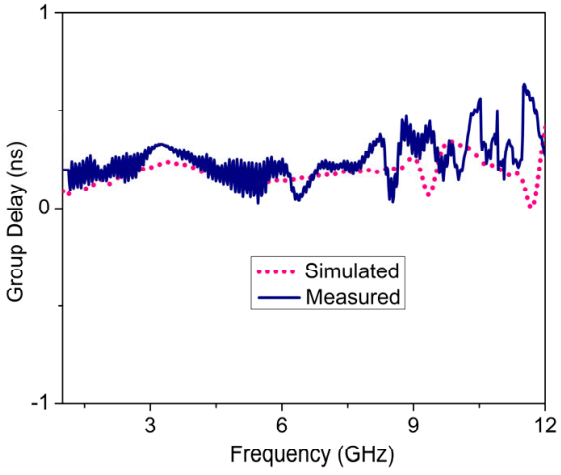

FIGURE 8. Simulated and measured group delay of proposed filter.

ing (9),

$$Q_e = \frac{\omega_0 \times \tau_{s_{11}(\omega_0)}}{4} \quad (9)$$

where $\tau_{S_{11}(\omega_0)}$ represents the group delay at the passband mid-frequency (ω_0). The measured group delay varies from 0.25 ns to 0.5 ns in the passband. The maximum variation is observed near the passband edges.

4. CONCLUSION

A compact UWB bandpass filter, realized with a combination of dual-split square complementary split ring resonator (DSS-CSRR) and substrate-integrated waveguide, is presented in this work. DSS-CSRRs are etched on the top and bottom layers to produce a wide bandwidth of 7.2 GHz. Slots are etched in the ground layer to improve the filter's performance characteristics by creating a transmission zero at the upper stopband. The measured results exhibit good passband characteristics with an insertion loss of less than 1.5 dB. The proposed filter contributes low insertion loss, ultra-wideband, and compact size. Moreover, it provides high stopband attenuation. Hence, the proposed filter is suitable for space applications.

REFERENCES

[1] Bandyopadhyay, A., P. Sarkar, and R. Ghatak, "A bandwidth reconfigurable bandpass filter for ultrawideband and wideband applications," *IEEE Transactions on Circuits and Systems II: Express Briefs*, Vol. 69, No. 6, 2747–2751, 2022.

[2] Bandyopadhyay, A., P. Sarkar, T. Mondal, and R. Ghatak, "A dual function reconfigurable bandpass filter for wideband and tri-band operations," *IEEE Transactions on Circuits and Systems II: Express Briefs*, Vol. 68, No. 6, 1892–1896, 2020.

[3] Che, W., C. Li, K. Deng, and L. Yang, "A novel bandpass filter based on complementary split rings resonators and substrate integrated waveguide," *Microwave and Optical Technology Letters*, Vol. 50, No. 3, 699–701, 2008.

[4] Falcone, F., T. Lopetegi, J. D. Baena, R. Marques, F. Martin, and M. Sorolla, "Effective negative-/spl epsiv/stopband microstrip lines based on complementary split ring resonators," *IEEE Microwave and Wireless Components Letters*, Vol. 14, No. 6, 280–282, 2004.

[5] Dong, Y. D., T. Yang, and T. Itoh, "Substrate integrated waveguide loaded by complementary split-ring resonators and its applications to miniaturized waveguide filters," *IEEE Transactions on Microwave Theory and Techniques*, Vol. 57, No. 9, 2211–2223, 2009.

[6] Muchhal, N. and S. Srivastava, "Design of miniaturized diamond shaped substrate integrated waveguide CSRR band pass filter for X band applications," in *2019 International Conference on Signal Processing and Communication (ICSC)*, 113–116, 2019.

[7] Kumar, R. and S. N. Singh, "Compact substrate integrated waveguide multiband band pass filter using octagonal complementary split ring resonators," *International Journal of Applied Engineering Research*, Vol. 12, No. 20, 10 127–10 133, 2017.

[8] Chen, R. S., S.-W. Wong, L. Zhu, and Q.-X. Chu, "Wideband bandpass filter using U-slotted substrate integrated waveguide (SIW) cavities," *IEEE Microwave and Wireless Components Letters*, Vol. 25, No. 1, 1–3, 2014.

[9] Zhan, X., Z. Tang, Y. Wu, and B. Zhang, "Substrate integrated waveguide dual-mode, dual-band filter," *Microwave Journal*, Vol. 57, No. 3, 94–102, 2014.

[10] Sarkar, D., T. Moyra, and L. Murmu, "An ultra-wideband (UWB) bandpass filter with complementary split ring resonator for coupling improvement," *AEU — International Journal of Electronics and Communications*, Vol. 71, 89–95, 2017.

[11] Li, Q. and T. Yang, "Compact UWB half-mode SIW bandpass filter with fully reconfigurable single and dual notched bands," *IEEE Transactions on Microwave Theory and Techniques*, Vol. 69, No. 1, 65–74, 2020.

[12] Huang, L., Y. Yuan, Y. Jiang, and N. Yuan, "Compact and high-performance UWB bandpass filter based on HMSIW," *Electronics Letters*, Vol. 56, No. 22, 1181–1183, 2020.

[13] Sazid, M. and N. S. Raghava, "Planar UWB-bandpass filter with multiple passband transmission zeros," *AEU — International Journal of Electronics and Communications*, Vol. 134, 153711, 2021.

[14] Pendry, J. B., A. J. Holden, D. J. Robbins, and W. J. Stewart, "Magnetism from conductors and enhanced nonlinear phenomena," *IEEE Transactions on Microwave Theory and Techniques*, Vol. 47, No. 11, 2075–2084, 1999.